Supporting Information

Modulating the band gap of pyrazinoquinoxaline-based metal-organic framework through orbital hybridization for enhanced visible light-driven C=N bond construction

Zitong Chen[†b], Linghui Cao[†b], Aogang Liu[b], Pengda Liu[b], Yuan Chen[*b], Juntao Yan[*a], Bao Li[*a, b]

[a]College of Chemistry and Environmental Engineering, Wuhan Polytechnic University, Wuhan 430023, China; Email: yanjuntaonihao@163.com.

[b]Key Laboratory of Material Chemistry for Energy Conversion and Storage, Semiconductor Chemistry Center, School of Chemistry and Chemical Engineering, Hubei Key Laboratory of Bioinorganic Chemistry & Materia Medica, Huazhong University of Science and Technology, Wuhan, Hubei 430074, People's Republic of China; Email: chenyuan122800@163.com; libao@hust.edu.cn.

Table of Contents

Materials and reagents

All the reagents and solvents were purchased commercially and directly used without further purification. Vitamin B_1 hydrochloride was provided by Shanghai Macklin Biochemical Technology Co., Ltd. Methyl 4-formylbenzoate, anhydrous indium (III) chloride ($InCl_3$), hydrobromic acid and 1,2,4,5-benzenetetramine tetrahydrochloride were obtained from Heowns Biochem Technologies, LLC, Tianjin. Sodium hydroxide (NaOH), hydrochloric acid (HCl) and triethylamine were acquired from Sinopharm Chemical Reagent Co., Ltd. Acetic acid and all the solvents were supplied by Shanghai Titan Scientific Co., Ltd. All the reagents for photocatalysis experiments were provided by the above-mentioned suppliers as well. Spin trapping agent 5,5-dimethyl-1-pyrroline N-oxide (DMPO) was obtained from Dojindo Laboratories.

Characterization and methods

The crystal structure of In-PQTB was obtained via Single-Crystal X-ray diffraction (SCXRD). Diffraction data for In-PQTB were collected via Bruker Venture at 100 K (Cu-Kα, λ = 1.54178 Å). The structure of In-PQTB was directly solved, and the non-hydrogen atoms were located from the trial structure and then refined anisotropically with SHELXTL using a full-matrix least squares procedure based on F^2 values. The hydrogen atom positions were fixed geometrically at calculated distances and allowed to ride on the parent atoms. Attempts to define the highly disordered solvent molecules were unsuccessful, thus the structure was refined with the PLATON "SQUEEZE" procedure. Supplementary crystallographic data and data under different temperatures for this paper can be obtained free of charge from CCDC-2358840 in Cambridge Crystallographic Data Centre via http://www.ccdc.cam.ac.uk/datarequest/cif.

The crystal and chemical structures of the samples were verified by X-ray diffraction (XRD, SmartLab-SE, Cu-K_α) and Fourier transform infrared spectroscopy (FT-IR, VERTEX 70, KBr pellet method). The thermostability of the samples were assessed by thermogravimetry (TG, Diamond TG/DTA) from room temperature to 800°C with a heating rate of 10°C/min under N_2 atmosphere. The light adsorption capacity of the samples was evaluated through solid-state ultraviolet-visible diffuse reflectance

spectroscopy (UV-vis-DRS, UV-3600, $BaSO_4$ as reference). The fluorescence spectra of the samples were obtained by RF-6000. Electron paramagnetic resonance (EPR, EMXmicro-6/1/P/L) was conducted to verify the formation of reactive oxygen species through irradiation of the samples. Nuclear magnetic resonance (NMR, Avance III, 400MHz) was employed to analyze the photocatalysis results. The morphology and element composition of the samples were identified by scanning electron microscopy/energy dispersive spectroscopy (SEM/EDS, Hitachi S-4800) and X-ray photoelectron spectroscopy (XPS, Thermo escalab 250XI). By-products and intermediates of the reactions were detected with mass spectrum (MS, microTOF II).

The photoelectric properties of the samples were assessed by electrochemical tests on the electrochemical workstation (CHI-760E, Shanghai Chenhua Instrument Co., Ltd.). A three-electrode system were applied, with the Ag/AgCl (saturated KCl) electrode as the reference electrode, a platinum foil as the counter electrode. To assemble the working electrode, 2 mg of the samples were dispersed into 25 μL of Nafion (5%) and 475 μL of ethanol absolute. After thorough ultrasonication of the suspension, 200 μL of the mixture was carefully let to drip dropwise on an area of 1 cm × 1 cm on an indium tin oxide (ITO) conductive glass. After dried at 50°C for 4 h, it was applied as the working electrode. Na_2SO_4 aqueous solution (1 mol/L) was employed as the electrolyte solution. The photocurrent was recorded at open circuit potential (OCP). The electrochemical impedance spectroscopy (EIS) was conducted in the frequency range of 10^{-2}~10^5 Hz with an amplitude of 5 mV at OCP. The Mott-Schottky curves were obtained from impedance-potential functions measured in the range of (OCP ± 1 V) with an amplitude of 5 mV and an increment of 20 mV.

Theoretical calculations were carried out based on previous reports. The structures of intermediates were optimized by $Dmol^3$ module, following by the frequency calculation to obtain zero-point vibration energy and Gibbs free energy. The generalized gradient approximation (GGA) with the Perdew-Burke-Ernzerhof (PBE, Phys. Rev. Lett. 1996, 77, 3865) function was employed. The convergence tolerance of energy, force and displacement convergence were set as 1×10^{-5} Ha, 2×10^{-3} Ha and 5×10^{-3} Å, respectively.

The core treatment and the electron treatment were performed by effective core potential (ECP) and double numerical plus d-functions (DNP) basis set, respectively.

Synthesis of H_4PQTB

The ligand H_4PQTB was synthesized based on the literature[1-4]. The synthetic route is shown in Scheme S1.

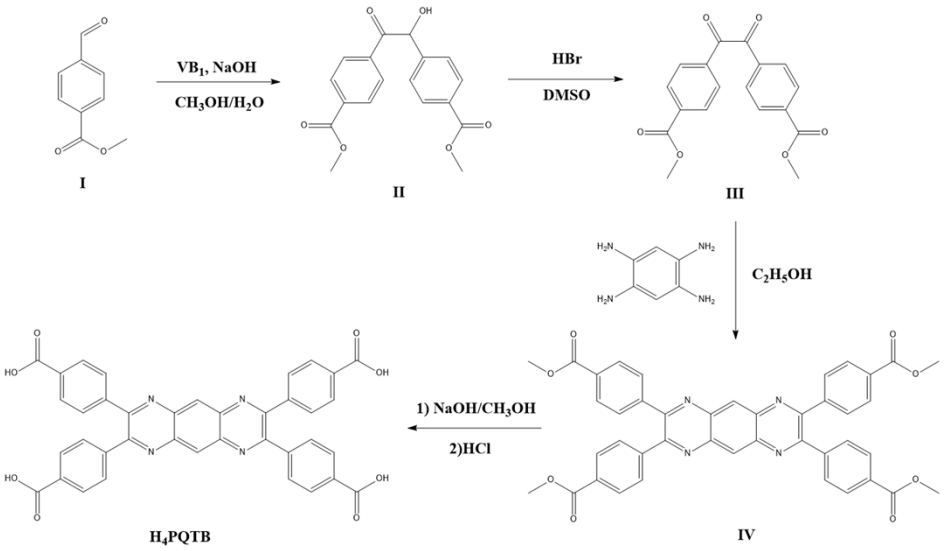

Scheme S1 Synthetic route of H_4PQTB.

*Synthesis of **II***

Vitamin B_1 hydrochloride (VB_1, $C_{12}H_{17}ClN_4OS{\cdot}HCl$, 337.27 g/mol, 5.35 mmol, 1.80 g) was dissolved into a mixed solution (H_2O:CH_3OH = 15 mL:45 mL). The mixture was cooled under ice bath and 5 mL of NaOH aqueous solution (2 mol/L) was slowly added under stirring. After stirring for 10 min, the ice bath was removed to recover room temperature. Then, methyl 4-formylbenzoate (**I**, $C_9H_8O_3$, 164.16 g/mol, 91 mmol, 14.9 g) was added. The mixture was heated to reflux at 80°C for 6 h. White solid **II** was obtained after filtered, washed with distilled water and methanol in turn and dried at 70°C overnight.

*Synthesis of **III***

II ($C_{18}H_{16}O_6$, 328.32 g/mol, 22.5 mmol, 7.4 g) was dissolved into dimethyl sulfoxide (DMSO, 51 mL), then 10.5 mL of hydrobromic acid (HBr, 48%) was slowly added. The mixture was heated to 70°C and kept for 24 h, then it was poured into abundant

distilled water. After filtered, washed with distilled water and dried at 70°C overnight, yellow solid **III** was obtained.

*Synthesis of **IV***

III ($C_{18}H_{14}O_6$, 326.30 g/mol, 7.20 mmol, 2.35 g) and 1,2,4,5-benzenetetramine tetrahydrochloride ($C_6H_{10}N_4 \cdot 4HCl$, 284.01 g/mol, 3.53 mmol, 1.00 g) were dissolved into 100 mL of absolute ethanol. Then, 0.5 mL of triethylamine (TEA) was added under stirring. After stirring for 5 min, 1.0 mL of acetic acid was added. The mixture was heated to reflux at 80°C for 24 h. Green precipitate **IV** was obtained after filtered, washed with absolute ethanol and dried at 70°C overnight.

*Synthesis of **H_4PQTB***

IV ($C_{42}H_{30}N_4O_8$, 718.72 g/mol, 2 g) and NaOH (4 g) was dissolved into 100 mL of methanol. The mixture was heated to reflux at 70 °C for 24 h. After evaporation, abundant distilled water was added to dissolve the solid. The precipitate was generated by adding HCl to adjust the pH of the solution to 3. The mixture was filtered, washed with distilled water and dried at 70°C overnight to yield brown solid **H_4PQTB**.

Preparation of In-PQTB

In-PQTB was synthesized through a typical solvothermal method. Initially, 10 mg of $InCl_3$ was dissolved into 3 mL of N, N-dimethylacetamide (DMF). Then, the solution was added into a Pyrex vial (5 mL) after 20 mg of H_4PQTB. The vessel was sealed with tinfoil and the mixture was treated with ultrasonication. The vial was heated to 120°C and kept for 72 h. Olive-shaped dark crystals were obtained after centrifugation. The solid was washed with DMF and dried at room temperature with filter papers.

Supporting figures and tables

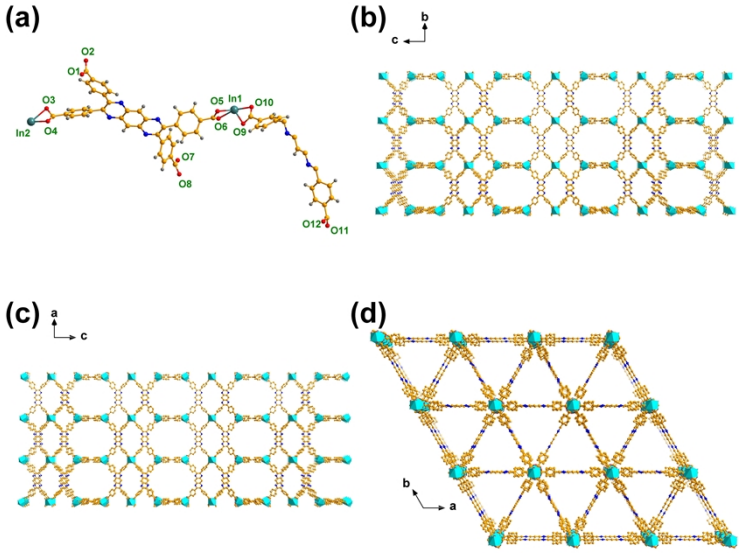

Figure S1 (a) Asymmetric unit of In-PQTB; (b-d) partial perspective view of the 3D packing structure of In-PQTB along *a*-axis, *b*-axis and *c*-axis, respectively.

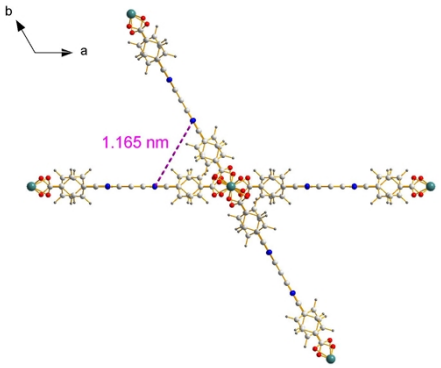

Figure S2 Distance between adjacent pyrazinoquinoxaline rings.

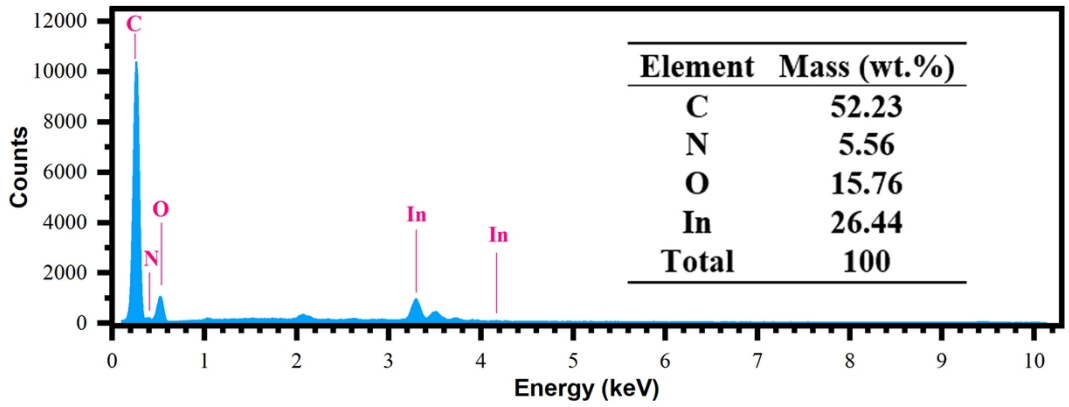

Figure S3 EDS image of In-PQTB.

Table S1. Crystal data of In-PQTB.

	In-PQTB
Empirical formula	$C_{114}H_{54}In_{2.05}N_{12}O_{24}$
Formula weight	2211.49
Temperature/K	173(2)
Crystal system	trigonal
Space group	P-3
a/Å	20.318(4)
b/Å	20.318(4)
c/Å	34.047(11)
α/°	90
β/°	90
γ/°	120
Volume/Å^3	12173(7)
Z	1
ρ_{calc}g/cm^3	0.302
μ/mm^{-1}	0.097
F(000)	1115.0
Crystal size/mm^3	0.2 × 0.1 × 0.1
Radiation	synchrotron (λ = 0.67012)
2θ range for data collection/°	2.456 to 44.16
Index ranges	-22 ≤ h ≤ 22, -22 ≤ k ≤ 22, -38 ≤ l ≤ 37
Reflections collected	114238
Independent reflections	11784 [R_{int}= 0.1533, R_{sigma}= 0.0806]
Data/restraints/parameters	11784/863/575
Goodness-of-fit on F^2	1.156
Final *R* indexes [$I \geq 2\sigma(I)$]	R_1= 0.1832, wR_2= 0.4204
Final *R* indexes [all data]	R_1= 0.2225, wR_2= 0.4399
Largest diff. peak/hole / e Å^{-3}	1.60/-0.67

Table S2. Bond lengths of In-PQTB.

Atom	Atom	Length/Å	Atom	Atom	Length/Å
In2	C36	2.582(15)	C42	C43	1.3900
In2	O3	2.309(19)	C43	C44	1.3900
In2	O4	2.34(2)	C43	C46	1.497(7)
In1	C46	2.580(12)	C44	C45	1.3900
In1	O5	2.221(9)	C46	O5	1.265(9)
In1	O6	2.259(9)	C46	O6	1.263(9)
In1	C56_1	2.656(14)	C50	C51	1.3900

In1	O8_1	2.279(10)	C50	C55	1.3900
In1	O7_1	2.285(10)	C50	C12	1.488(10)
N1	C2	1.3900	C51	C52	1.3900
N1	C6	1.3900	C52	C53	1.3900
C2	C3	1.3900	C53	C54	1.3900
C2	C30	1.492(9)	C53	C56	1.493(7)
C3	N4	1.3900	C54	C55	1.3900
C3	C21	1.478(9)	C56	O7	1.248(9)
N4	C5	1.3900	C56	O8	1.267(9)
C5	C6	1.3900	N3	C12	1.384(4)
C5	C10	1.3900	C11	C12	1.376(8)
C6	C7	1.3900	C11	N2	1.391(7)
C7	C8	1.3900	O3_1	C36_1	1.287(10)
C8	C9	1.3900	C36_1	O4_1	1.295(11)
C8	N3	1.387(4)	C36_1	C33_1	1.526(11)
C9	C10	1.3900	C33_1	C32_1	1.394(5)
C9	N2	1.386(6)	C33_1	C34_1	1.392(5)
C21	C22	1.3900	C32_1	C31_1	1.393(5)
C21	C26	1.3900	C31_1	C30_1	1.392(5)
C22	C23	1.3900	C30_1	C35_1	1.393(5)
C23	C24	1.3900	C30_1	C2_1	1.499(10)
C24	C25	1.3900	C35_1	C34_1	1.391(5)
C24	C27	1.494(7)	C2_1	N1_1	1.3899(3)
C25	C26	1.3900	N1_1	C6_1	1.3895(2)
C27	O1	1.228(8)	C6_1	C7_1	1.3924(3)
C27	O2	1.287(8)	C7_1	C8_1	1.3900(2)
C30	C31	1.3900	C8_1	N3_1	1.3854(3)
C30	C35	1.3900	N3_1	C12_1	1.3868(3)
C31	C32	1.3900	C12_1	C50_1	1.499(10)
C32	C33	1.3900	C50_1	C55_1	1.396(5)
C33	C34	1.3900	C50_1	C51_1	1.395(5)
C33	C36	1.525(9)	C55_1	C54_1	1.393(5)
C34	C35	1.3900	C54_1	C53_1	1.394(5)
C36	O3	1.287(9)	C53_1	C52_1	1.393(5)
C36	O4	1.294(9)	C53_1	C56_1	1.487(8)
C40	C41	1.3900	C52_1	C51_1	1.394(5)
C40	C45	1.3900	C56_1	O8_1	1.265(10)
C40	C11	1.486(8)	C56_1	O7_1	1.248(10)

C41	C42	1.3900	

Table S3. Bond angles of In-PQTB.

Atom	Atom	Atom	Angle/°	Atom	Atom	Atom	Angle/°
O3	In2	C36	29.8(3)	C44	C43	C46	119.8(4)
O3	In2	O4	55.5(4)	C45	C44	C43	120.0
O4	In2	C36	30.0(3)	C44	C45	C40	120.0
C46	In1	C56_1	120.3(12)	C43	C46	In1	170.0(11)
O5	In1	C46	29.4(2)	O5	C46	In1	59.4(5)
O5	In1	O6	58.2(3)	O5	C46	C43	117.5(8)
O5	In1	C56_1	105.8(12)	O6	C46	In1	61.1(5)
O5	In1	O8_1	121.2(16)	O6	C46	C43	118.6(9)
O5	In1	O7_1	93.0(15)	O6	C46	O5	119.0(11)
O6	In1	C46	29.3(2)	C46	O5	In1	91.3(6)
O6	In1	C56_1	134.3(10)	C46	O6	In1	89.5(6)
O6	In1	O8_1	162.0(11)	C51	C50	C55	120.0
O6	In1	O7_1	106.3(10)	C51	C50	C12	119.9(4)
O8_1	In1	C46	144.9(14)	C55	C50	C12	120.1(4)
O8_1	In1	C56_1	28.4(3)	C52	C51	C50	120.0
O8_1	In1	O7_1	56.0(4)	C53	C52	C51	120.0
O7_1	In1	C46	97.2(13)	C52	C53	C54	120.0
O7_1	In1	C56_1	28.0(3)	C52	C53	C56	119.6(4)
N1	C2	C3	120.0	C54	C53	C56	120.4(4)
N1	C2	C30	113.3(4)	C55	C54	C53	120.0
C3	C2	C30	126.1(5)	C54	C55	C50	120.0
C2	C3	C21	130.6(12)	O7	C56	C53	120.4(8)
N4	C3	C2	120.0	O7	C56	O8	119.2(9)
N4	C3	C21	108.8(13)	O8	C56	C53	118.0(8)
C5	N4	C3	120.0	C12	N3	C8	116.6(6)
N4	C5	C6	120.0	C12	C11	C40	124.6(6)
C5	C6	N1	120.0	C12	C11	N2	121.3(5)
C7	C6	N1	120.0	N2	C11	C40	112.2(6)
C7	C6	C5	120.0	N3	C12	C50	106.6(5)
C6	C7	C8	120.0	C11	C12	C50	130.4(6)
C7	C8	C9	120.0	C11	C12	N3	122.4(5)
N3	C8	C7	118.7(4)	C9	N2	C11	116.7(7)
N3	C8	C9	121.3(4)	C36	O3	In2	86.9(11)
C10	C9	C8	120.0	C36	O4	In2	85.4(11)

N2	C9	C8	121.8(5)	O3_1	C36_1	O4_1	112.7(13)
N2	C9	C10	118.2(5)	O3_1	C36_1	C33_1	126.7(16)
C9	C10	C5	120.0	O4_1	C36_1	C33_1	113.7(15)
C22	C21	C3	109.4(19)	C32_1	C33_1	C36_1	111.7(13)
C22	C21	C26	120.0	C34_1	C33_1	C36_1	128.2(16)
C26	C21	C3	130.6(19)	C34_1	C33_1	C32_1	118.9(6)
C23	C22	C21	120.0	C31_1	C32_1	C33_1	119.8(8)
C22	C23	C24	120.0	C30_1	C31_1	C32_1	119.2(9)
C23	C24	C25	120.0	C31_1	C30_1	C35_1	118.3(9)
C23	C24	C27	119.6(4)	C31_1	C30_1	C2_1	120.4(7)
C25	C24	C27	120.4(4)	C35_1	C30_1	C2_1	119.8(6)
C26	C25	C24	120.0	C34_1	C35_1	C30_1	120.0(7)
C25	C26	C21	120.0	C35_1	C34_1	C33_1	120.4(7)
O1	C27	C24	123.0(8)	N1_1	C2_1	C30_1	111.0(7)
O1	C27	O2	121.2(8)	C6_1	N1_1	C2_1	119.978(18)
O2	C27	C24	115.7(6)	N1_1	C6_1	C7_1	120.031(18)
C31	C30	C2	119.9(4)	C8_1	C7_1	C6_1	120.053(18)
C31	C30	C35	120.0	N3_1	C8_1	C7_1	119.422(18)
C35	C30	C2	120.1(4)	C8_1	N3_1	C12_1	118.527(19)
C30	C31	C32	120.0	N3_1	C12_1	C50_1	104.5(7)
C33	C32	C31	120.0	C55_1	C50_1	C12_1	119.0(6)
C32	C33	C36	111.9(12)	C51_1	C50_1	C12_1	119.3(7)
C34	C33	C32	120.0	C51_1	C50_1	C55_1	117.6(9)
C34	C33	C36	128.1(12)	C54_1	C55_1	C50_1	119.7(7)
C33	C34	C35	120.0	C55_1	C54_1	C53_1	119.7(8)
C34	C35	C30	120.0	C54_1	C53_1	C56_1	120.8(6)
C33	C36	In2	167.1(11)	C52_1	C53_1	C54_1	118.0(6)
O3	C36	In2	63.3(10)	C52_1	C53_1	C56_1	121.1(6)
O3	C36	C33	125.7(15)	C53_1	C52_1	C51_1	119.7(7)
O3	C36	O4	114.2(10)	C52_1	C51_1	C50_1	119.5(8)
O4	C36	In2	64.7(11)	C53_1	C56_1	In1	179.2(9)
O4	C36	C33	113.6(12)	O8_1	C56_1	In1	59.0(6)
C41	C40	C45	120.0	O8_1	C56_1	C53_1	120.2(9)
C41	C40	C11	120.1(4)	O7_1	C56_1	In1	59.3(6)
C45	C40	C11	119.9(4)	O7_1	C56_1	C53_1	121.6(10)
C40	C41	C42	120.0	O7_1	C56_1	O8_1	117.0(12)
C43	C42	C41	120.0	C56_1	O8_1	In1	92.6(8)
C42	C43	C44	120.0	C56_1	O7_1	In1	92.7(8)

C42	C43	C46	120.2(4)

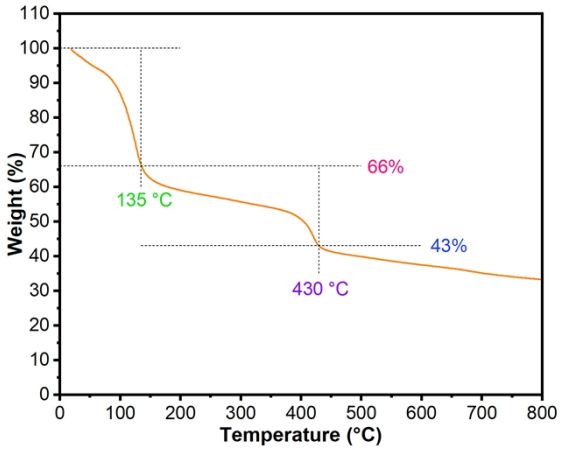

Figure S4 TG curve of In-PQTB.

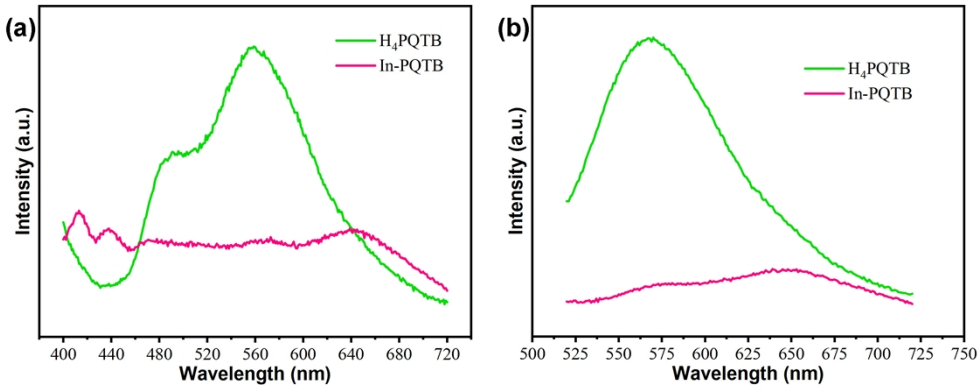

Figure S5 Solid-state fluorescence spectra of In-PQTB excited at (a) 380 nm and (b) 490 nm, respectively.

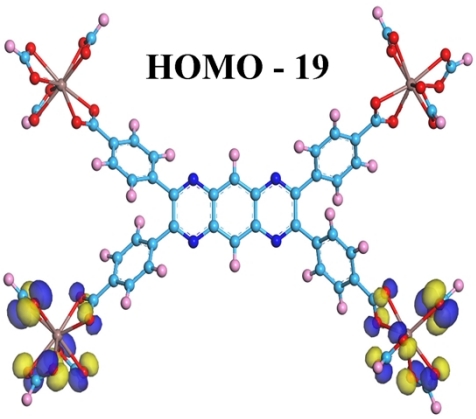

Figure S6 HOMO - 19 of In-PQTB.

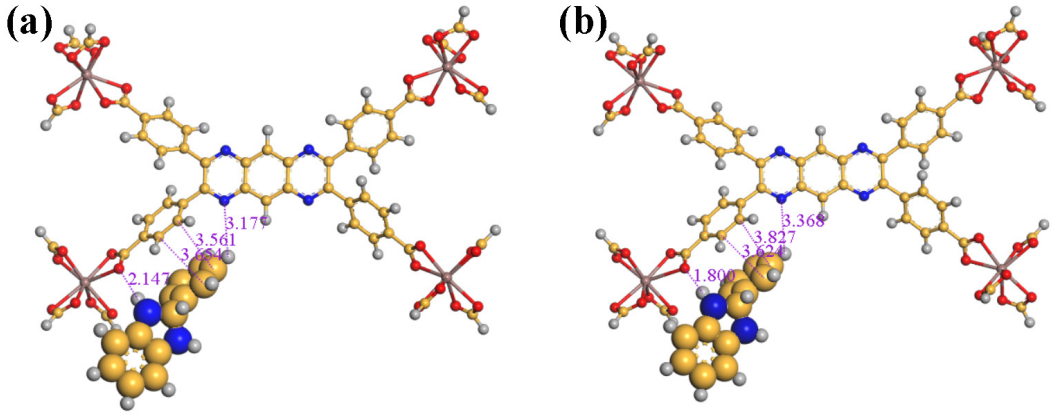

Figure S7 Distance among In-PQTB and (a) intermediate (**IV**) and (b) intermediate (**V**), respectively.

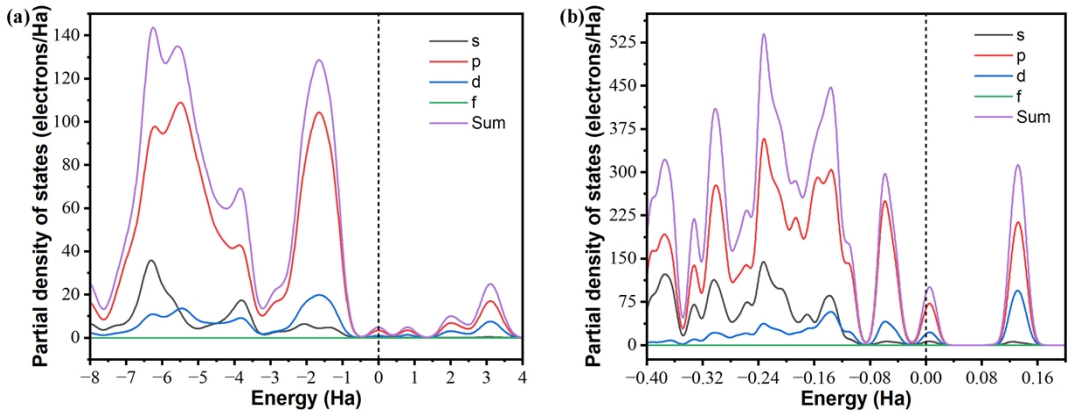

Figure S8 Partial density of states of In-PQTB interacting with (a) intermediate (**IV**) and (b) intermediate (**V**), respectively.

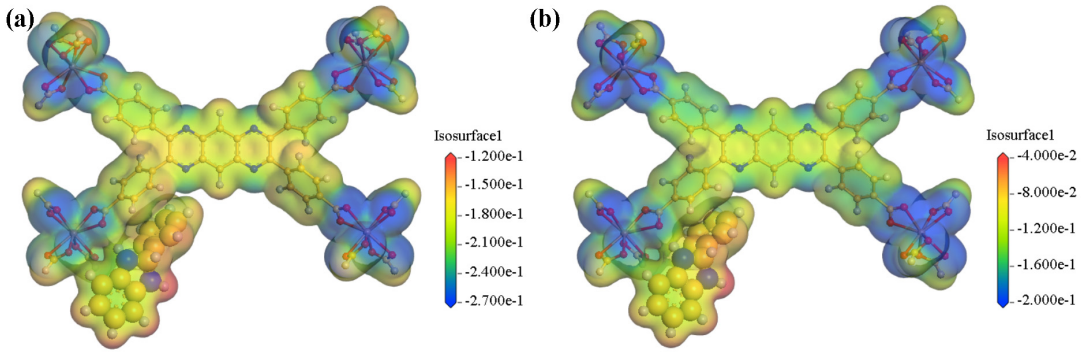

Figure S9 Images of electrostatic potential iso-surface of electron density of In-PQTB interacting with (a) intermediate (**IV**) and (b) intermediate (**V**), respectively.

Investigation of reaction mechanism

To verify the proposed mechanism, control experiments were carried out. For Reaction 2, with the addition of triethanolamine (TEOA) and *p*-benzoquinone (BQ) (2 equiv.), the yields for **5a** decrease to 44% and 17%, respectively, suggesting that superoxide radicals and holes have participated in the reaction process. By-products and intermediates for Reaction 2 were detected with NMR and mass spectrum. According to previous reports[5-10], characteristic peaks of by-product **B** can be observed (Figure S10 and S11).

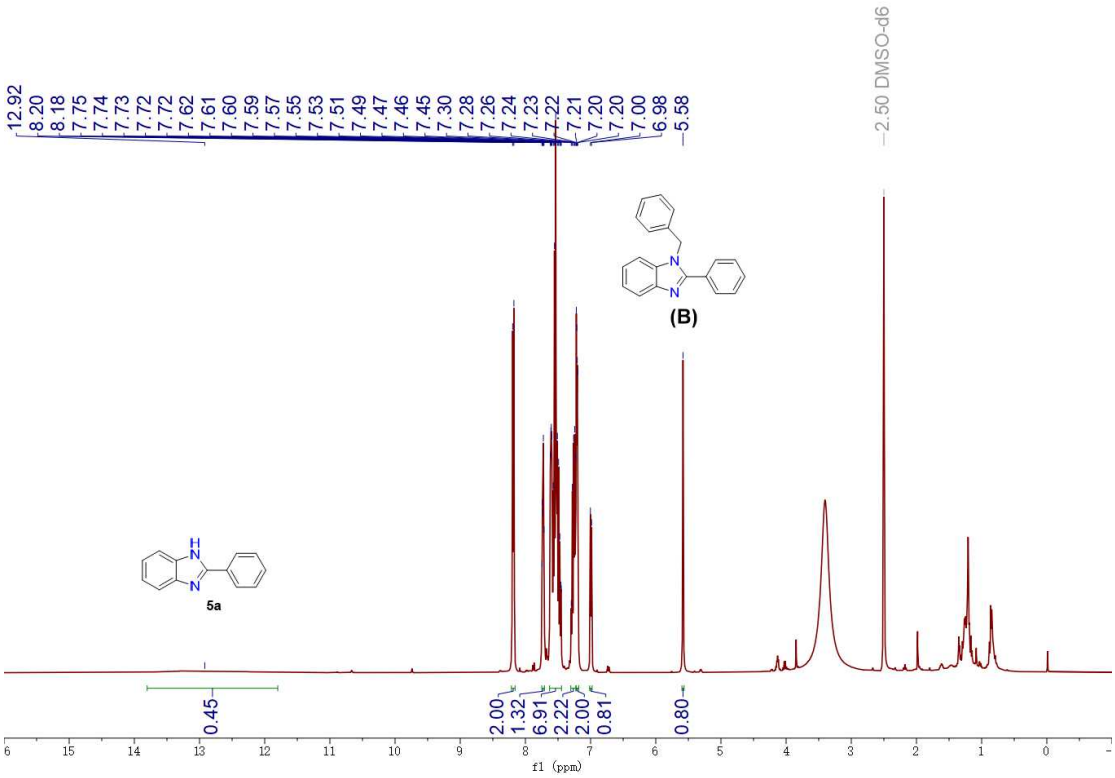

Figure S10 ^{1}H NMR spectrum of the mixture of **5a** and **B**.

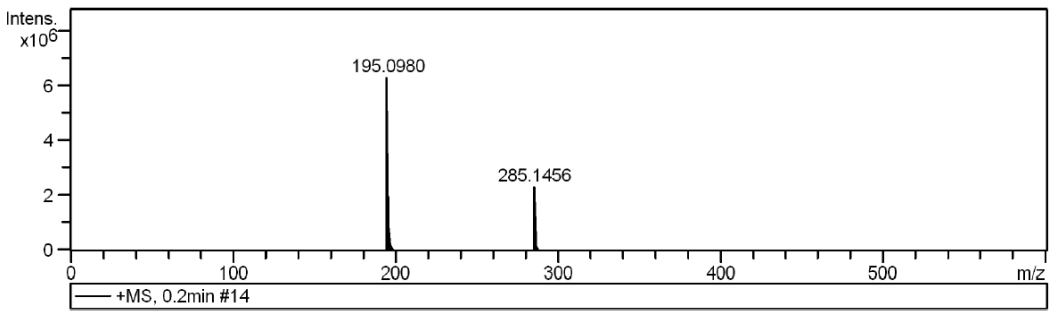

Figure S11 Mass spectrum of the mixture of **5a** and **B**. (Left: [**5a**+H^{+}]; Right: [**B**+H^{+}])

Evaluation of catalytic performance

The cycling stability of In-PQTB was checked by five consecutive catalytic cycles. As is depicted in Figure S12, the catalytic activity of In-PQTB slightly deteriorates after five runs, which guarantees its practical applications. Moreover, the catalytic activity of In-PQTB has been compared with those of other catalysts in terms of yields of **5a** (Table S4), indicating its superiority. The much higher yield of In-PQTB than that of the mixture of $InCl_3$ and H_4PQTB highlights the effect of coordination. The sequentially increasing yields of Zn-PQTB, Cd-PQTB and In-PQTB confirm the significance of MLCT process, energy level matching and orbital hybridization between metal nodes and ligands.

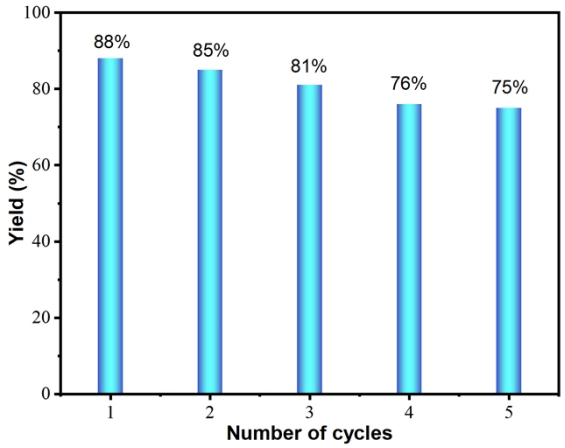

Figure S12 Cycling stability of In-PQTB.

Table S4. Comparison of photocatalytic performance of In-PQTB and other catalysts. (in terms of Reaction 2, yield of **5a**)

Catalysts	E_g	Dosage	Light Source	Yield
In-PQTB	1.474 eV	2.5 mol%	10 W white LED	88%
$InCl_3$ + H_4PQTB	—	Both 2.5 mol%	10 W white LED	28%
Zn-PQTB	2.93 eV	2.5 mol%	10 W 365 nm	31%
Cd-PQTB	2.38 eV	2.5 mol%	10 W white LED	53%
Rhodamine B[11]	—	2 mol%	10 W blue LED	49%
Cu-MOF[12]	2.01 eV	4 mol%	10 W 365 nm	25%
In-MOF[13]	2.44 eV	4 mol%	10 W 365 nm	45%

Characterization of products

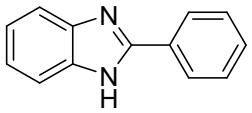

2-phenyl-1*H*-benzo[*d*]imidazole (**5a**)

^{1}H NMR (400 MHz, DMSO-d_6) δ 12.94 (s, 1H), 8.32 – 8.10 (m, 2H), 7.70 – 7.45 (m, 5H), 7.21 (dd, J = 6.1, 3.2 Hz, 2H).

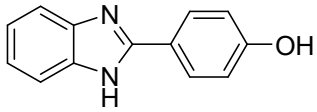

4-(1*H*-benzo[*d*]imidazol-2-yl)phenol (**5b**)

^{1}H NMR (400 MHz, DMSO-d_6) δ 12.65 (s, 1H), 9.96 (s, 1H), 8.00 (d, J = 8.3 Hz, 2H), 7.60 – 7.45 (m, 2H), 7.15 (dd, J = 6.1, 3.2 Hz, 2H), 6.91 (d, J = 8.3 Hz, 2H).

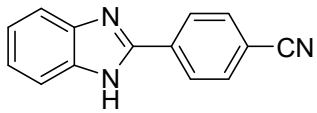

4-(1*H*-benzo[*d*]imidazol-2-yl)benzonitrile (**5c**)

^{1}H NMR (400 MHz, DMSO-d_6) δ 13.19 (s, 1H), 8.34 (d, J = 8.2 Hz, 2H), 7.99 (d, J = 8.3 Hz, 2H), 7.65 (s, 2H), 7.25 (dd, J = 6.1, 3.1 Hz, 2H).

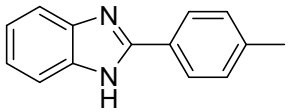

2-(*p*-tolyl)-1*H*-benzo[*d*]imidazole (**5d**)

^{1}H NMR (400 MHz, DMSO-d_6) δ 12.84 (s, 1H), 8.08 (d, J = 8.0 Hz, 2H), 7.59 (dd, J = 6.0, 3.2 Hz, 2H), 7.35 (d, J = 7.9 Hz, 2H), 7.19 (dd, J = 6.0, 3.2 Hz, 2H), 2.37 (s, 3H).

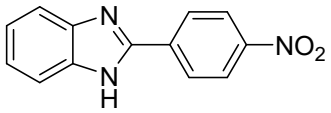

2-(4-nitrophenyl)-1*H*-benzo[*d*]imidazole (**5e**)

^{1}H NMR (400 MHz, DMSO-d_6) δ 13.32 (s, 1H), 8.42 (s, 4H), 7.68 (d, J = 8.0 Hz, 2H), 7.27 (dd, J = 6.1, 3.1 Hz, 2H).

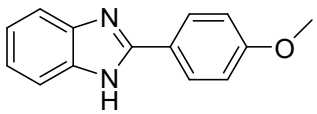

2-(4-methoxyphenyl)-1*H*-benzo[*d*]imidazole (**5f**)

^{1}H NMR (400 MHz, DMSO-d_6) δ 8.12 (d, J = 8.5 Hz, 2H), 7.56 (s, 2H), 7.21 – 7.07 (m, 4H), 3.83 (s, 3H).

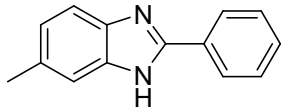

6-methyl-2-phenyl-1*H*-benzo[*d*]imidazole (**5g**)

^{1}H NMR (400 MHz, DMSO-d_6) δ 12.76 (s, 1H), 8.15 (d, J = 7.6 Hz, 2H), 7.60 – 7.42 (m, 4H), 7.37 (s, 1H), 7.02 (d, J = 8.2 Hz, 1H), 2.43 (s, 3H).

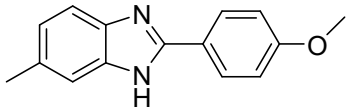

2-(4-methoxyphenyl)-6-methyl-1*H*-benzo[*d*]imidazole (**5h**)

^{1}H NMR (400 MHz, DMSO-d_6) δ 8.11 (d, J = 8.8 Hz, 2H), 7.44 (d, J = 8.1 Hz, 1H), 7.35 (s, 1H), 7.09 (d, J = 8.8 Hz, 2H), 6.99 (d, J = 8.1 Hz, 1H), 3.82 (s, 3H), 2.41 (s, 3H).

References

1. Y. Chen, A.-g. Liu, P.-d. Liu, Z.-y. Zhang, F. Yu, W. Qi and B. Li, *lnorg. Chem.*, 2022, **61**, 16009-16019.

2. S. Pizarro, M. Gallardo, C. Leyton, E. Castro, F. Gajardo and A. Delgadillo, *Spectrochim Acta A Mol Biomol Spectrosc*, 2015, **146**, 61-65.

3. I. Hisaki, N. Q. Emilya Affendy and N. Tohnai, *CrystEngComm*, 2017, **19**, 4892-4898.

4. A. G. Liu, X. Y. Meng, Y. Chen, Z. T. Chen, P. D. Liu and B. Li, *ACS Appl. Mater. Interfaces*, 2023, **16**, 669-683.

5. X. Huang, Y. He, Z. Chen and C. Hu, *Chin. J. Chem* . 2009, **27**, 1526-1530.

6. H. Sharma, N. Kaur, N. Singh and D. O. Jang, *Green Chem.*, 2015, **17**, 4263-4270.

7. P. Ghosh and A. Mandal, *Tetrahedron Letters*, 2012, **53**, 6483-6488.

8. E. S. paghaleh, S. M. Vahdat and M. Hatami, *J. Nanostruct.*, 2021, **11**, 286-296.

9. S. Azadi, A. R. Sardarian and M. Esmaeilpour, *Monatsh. Chem.*, 2023, **154**, 887-903.

10. R. Chebolu, D. N. Kommi, D. Kumar, N. Bollineni and A. K. Chakraborti, *J. Org. Chem.*, 2012, **77**, 10158-10167.

11. Z. Li, H. Song, R. Guo, M. Zuo, C. Hou, S. Sun, X. He, Z. Sun and W. Chu, *Green Chem.*, 2019, **21**, 3602-3605.

12. X. Chen, Z.-t. Chen, F. Zhu, Y. Chen, A.-g. Liu, X. Yin, Z.-k. Chen and B. Li, *CrystEngComm*, 2024, **26**, 4489-4497.

13. Y. Chen, X. Yin, Z. K. Chen, P. M. Wang and B. Li, *lnorg. Chem.*, 2023, **62**, 10626-10634.

^{1}H NMR spectra of products

2a-^{1}H NMR (400 MHz, $CDCl_3$)

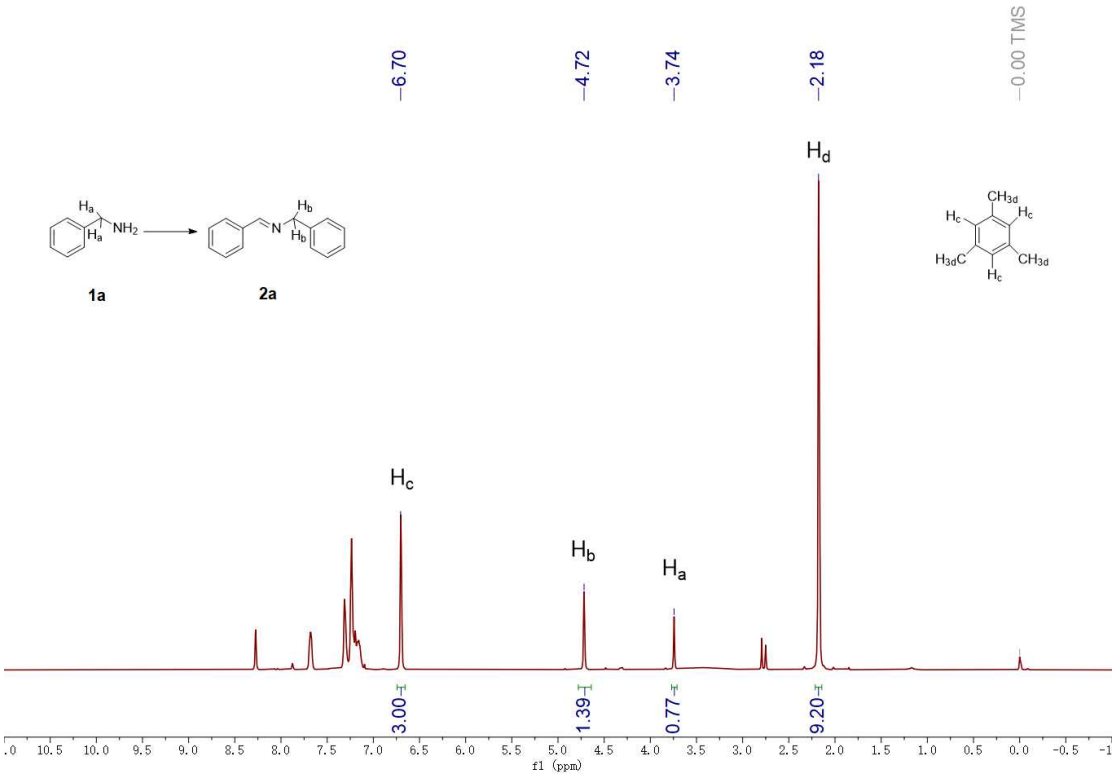

2b-^{1}H NMR (400 MHz, $CDCl_3$)

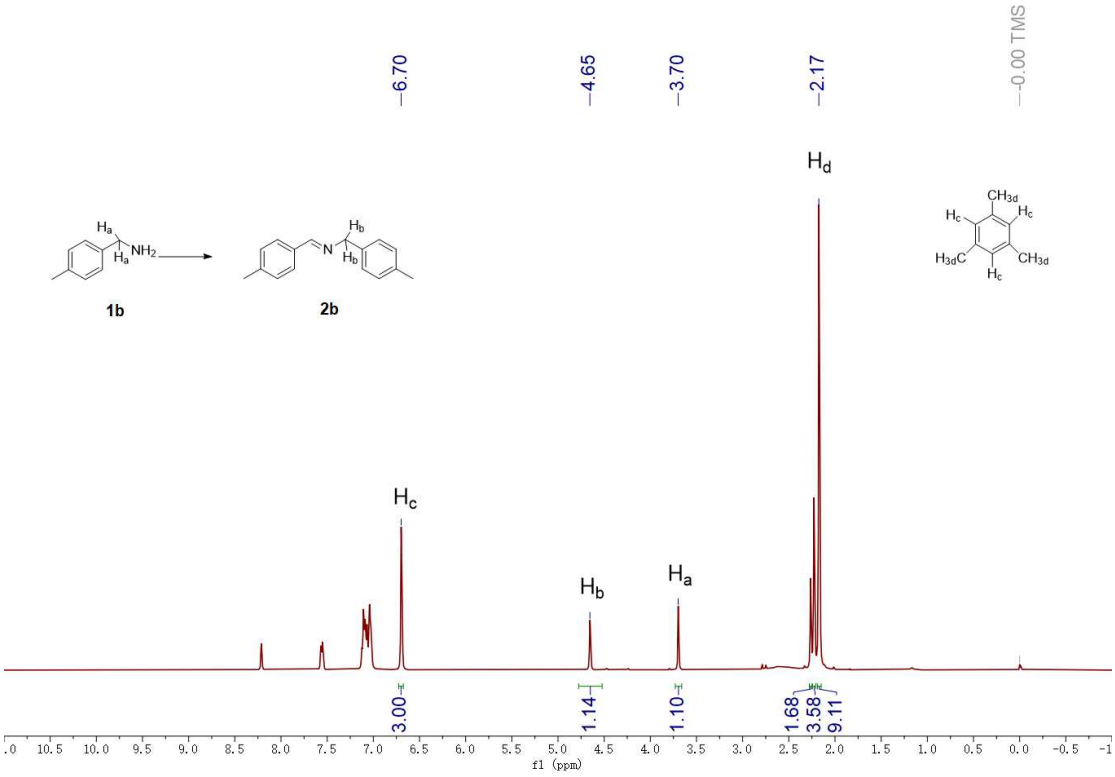

2c-^{1}H NMR (400 MHz, $CDCl_3$)

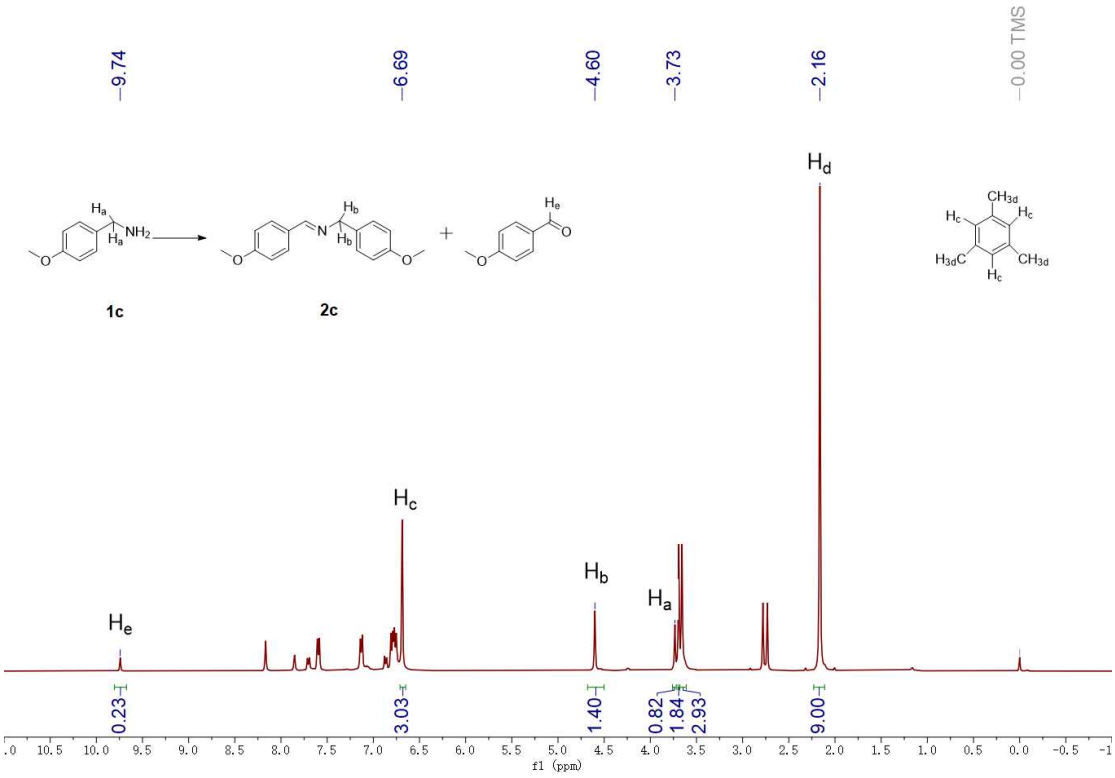

2d-^{1}H NMR (400 MHz, $CDCl_3$)

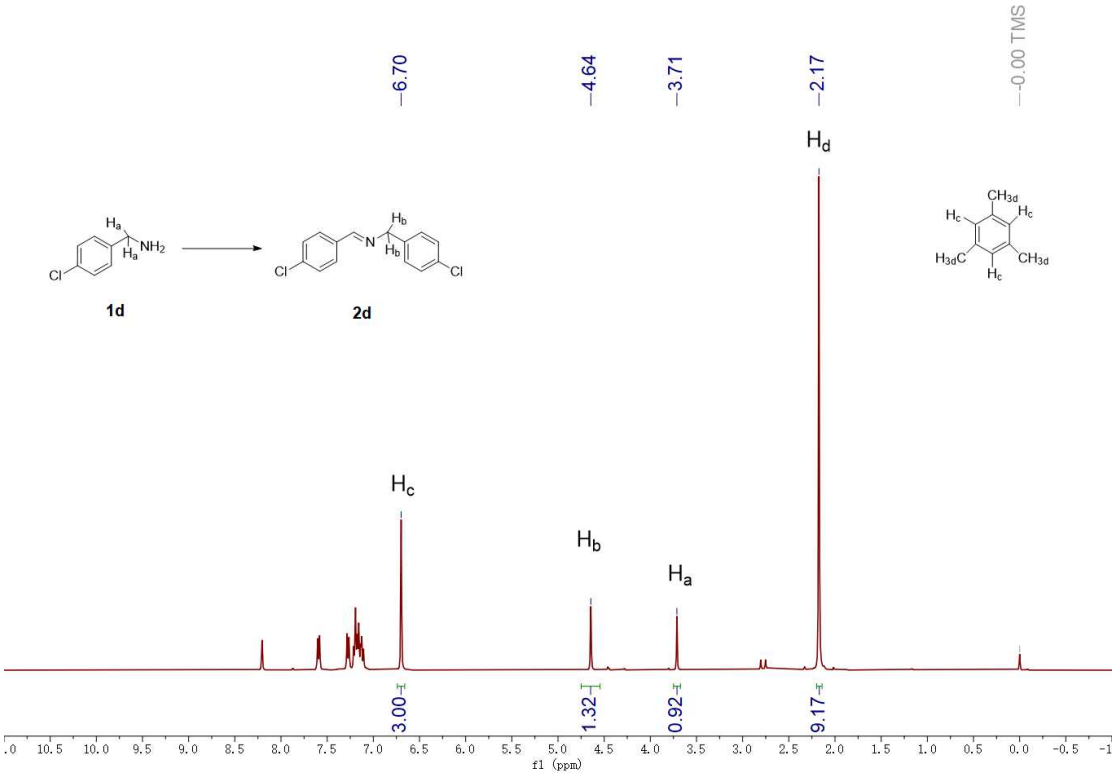

2e-^{1}H NMR (400 MHz, $CDCl_3$)

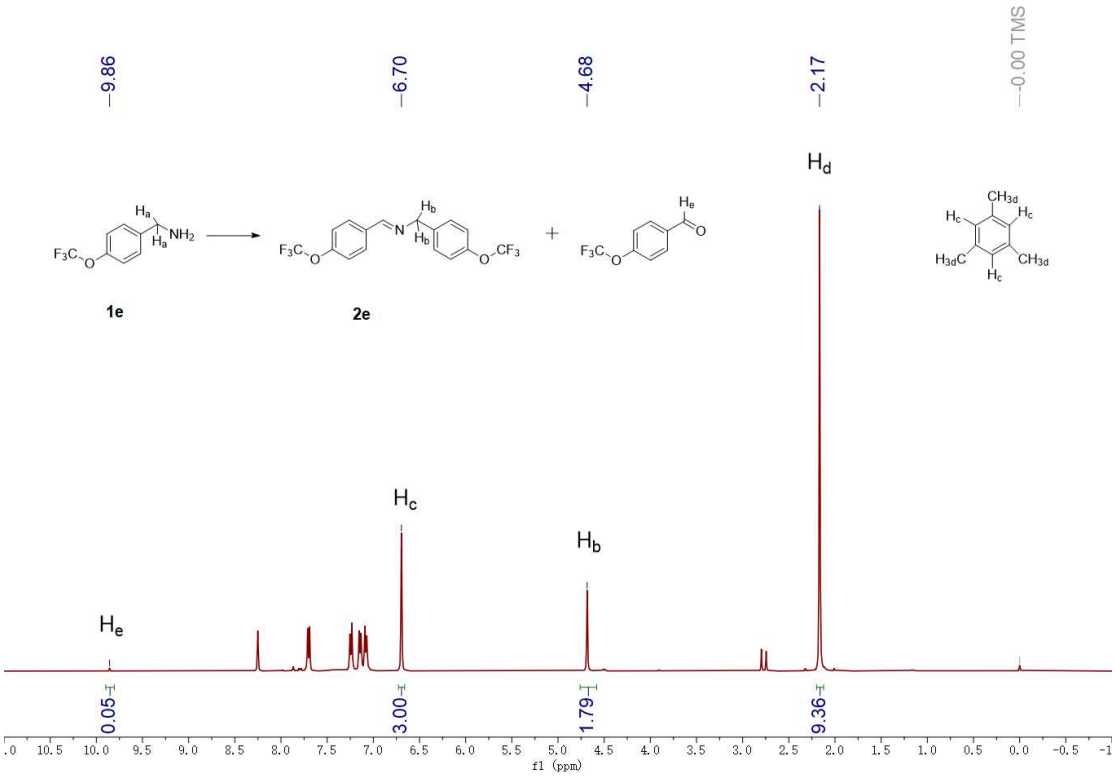

2f-^{1}H NMR (400 MHz, $CDCl_3$)

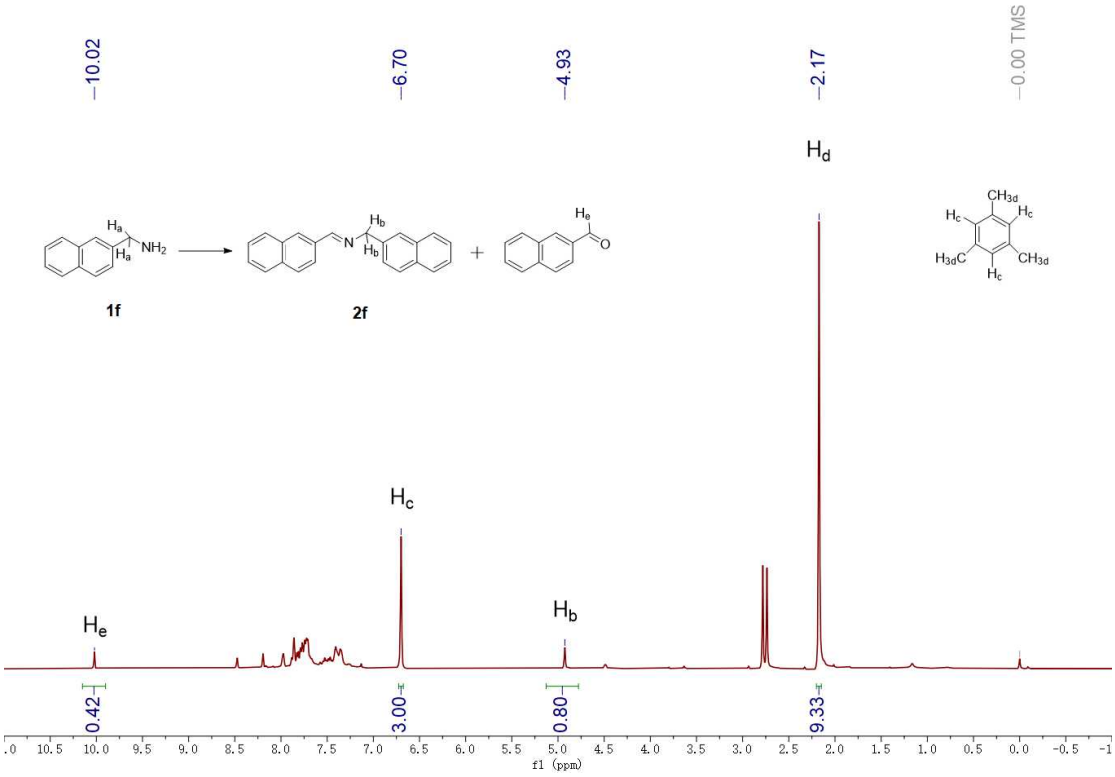

2g-^{1}H NMR (400 MHz, $CDCl_3$)

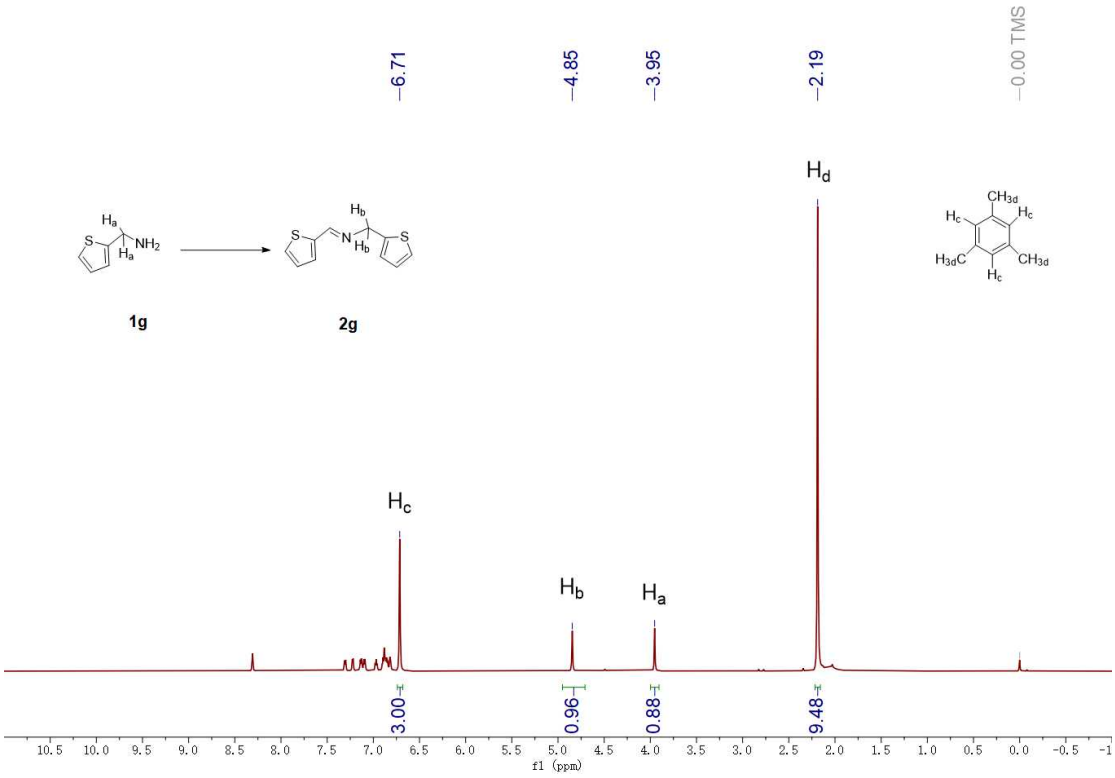

5a-^{1}H NMR (400 MHz, DMSO-d_6)

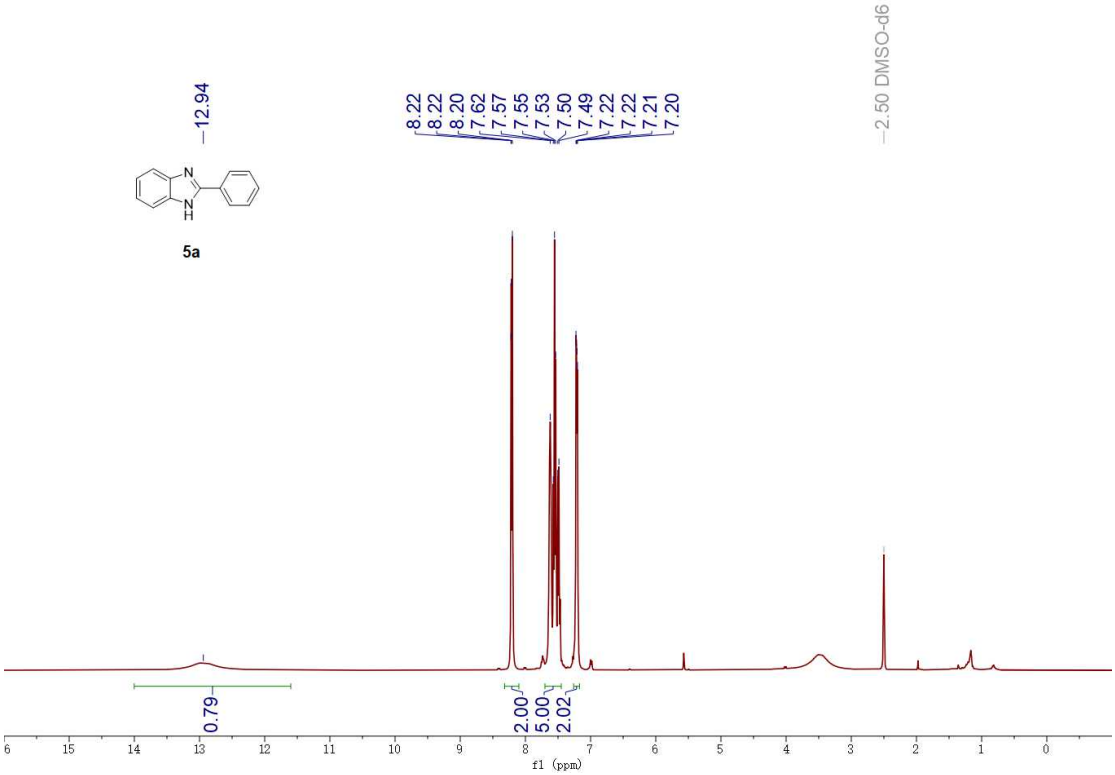

5b-^{1}H NMR (400 MHz, DMSO-d_6)

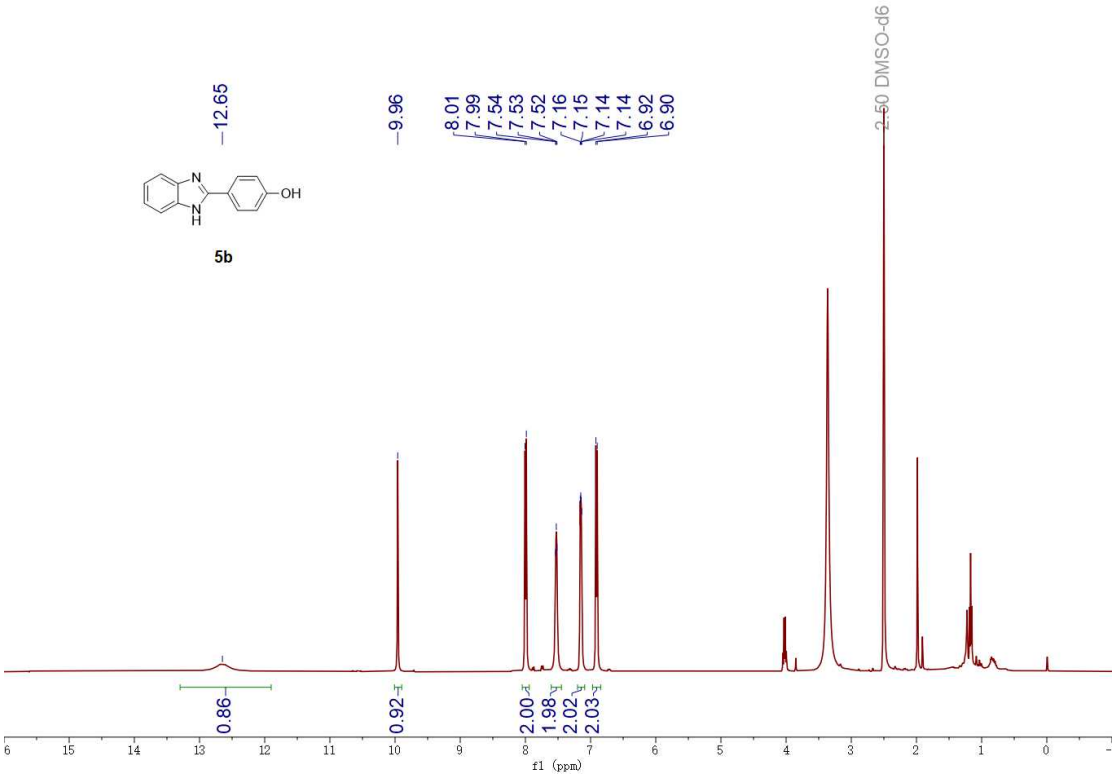

5c-^{1}H NMR (400 MHz, DMSO-d_6)

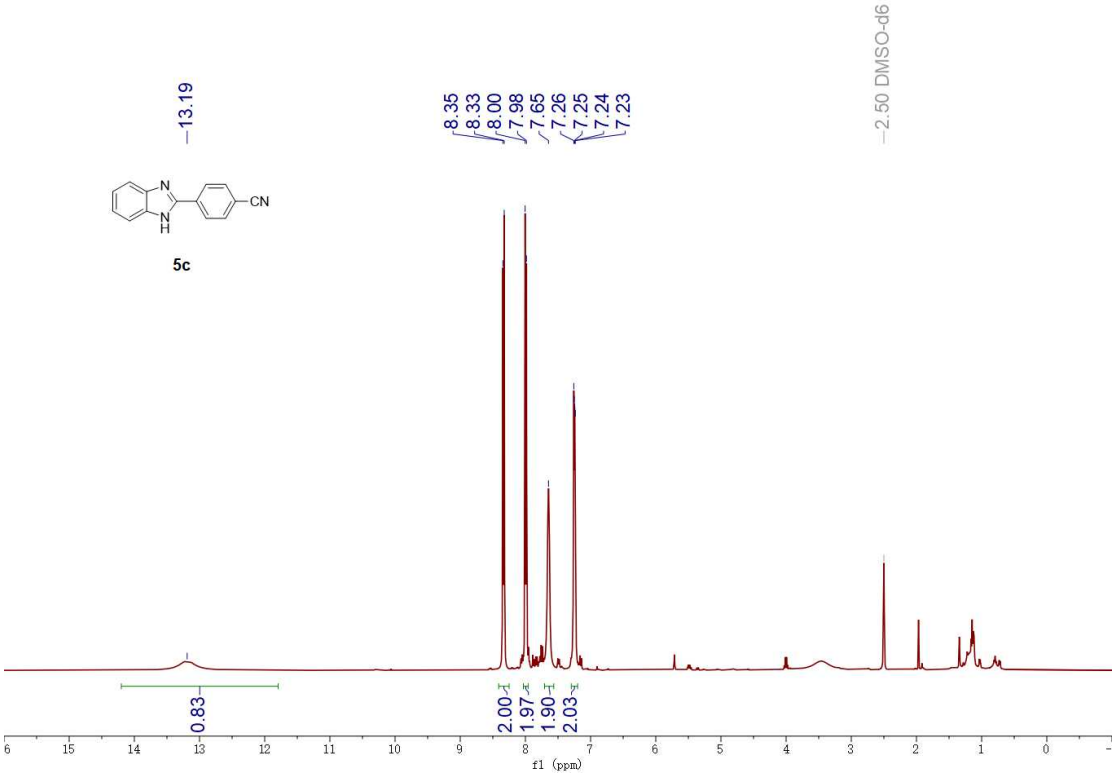

5d-^{1}H NMR (400 MHz, DMSO-d_6)

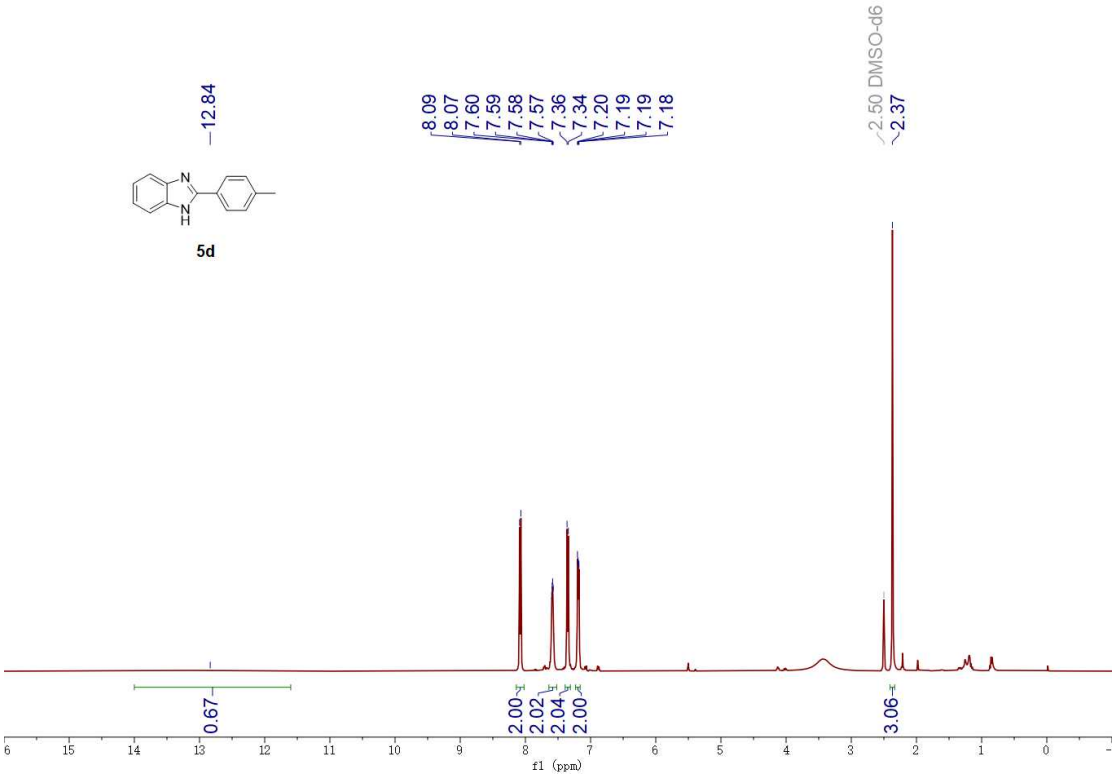

5e-^{1}H NMR (400 MHz, DMSO-d_6)

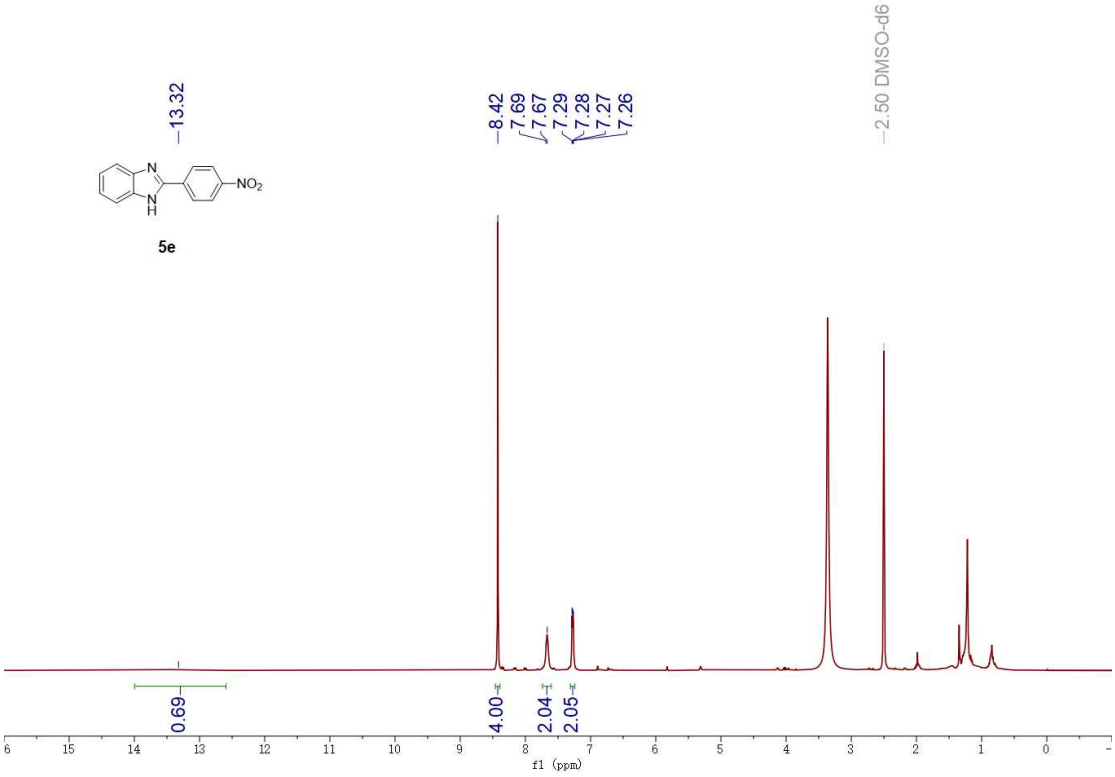

5f-^{1}H NMR (400 MHz, DMSO-d_6)

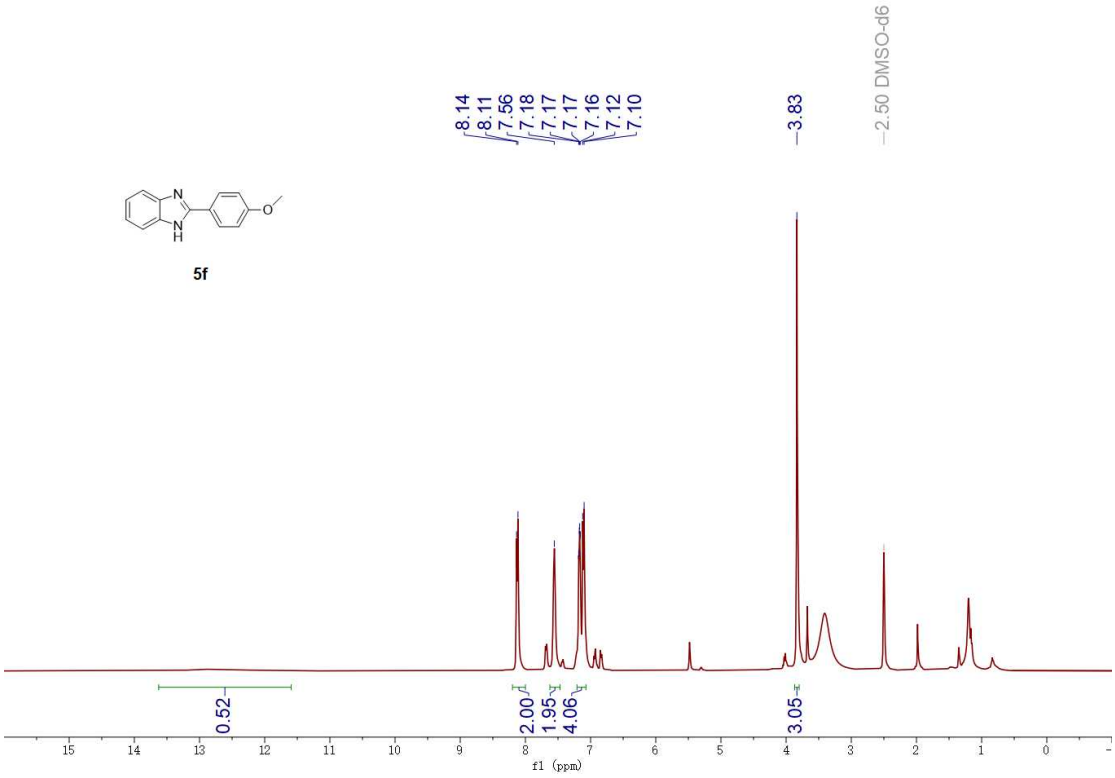

5g-^{1}H NMR (400 MHz, DMSO-d_6)

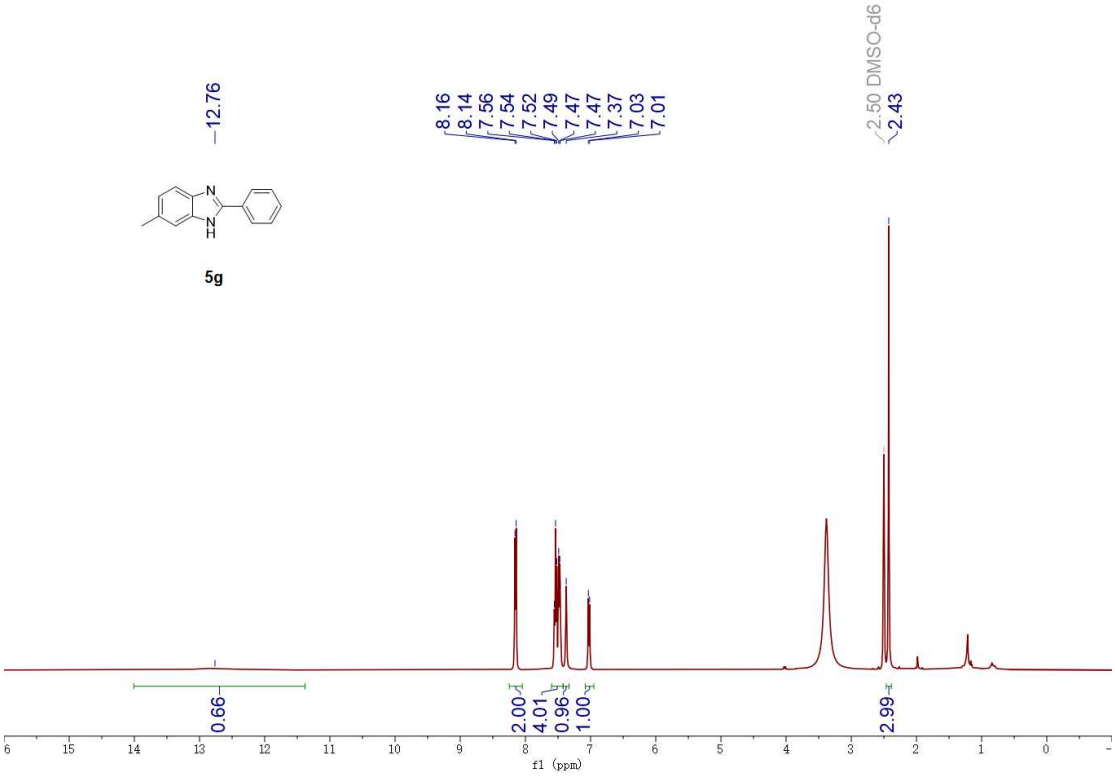

5h-^{1}H NMR (400 MHz, DMSO-d_6)